CHINESE OPTICS LETTERS

Vol. 20, No. 12 | December 2022

High-efficiency monolayer metallic metasurface for modulation of orbital angular momentum

Peijun Liu (刘佩军), Yanan Fu (付亚男), Xi Xie (谢 希), Changjun Min (闵长俊)*, Yuquan Zhang (张聿全), and Xiaocong Yuan (袁小聪)**

Nanophotonics Research Center, Shenzhen Key Laboratory of Micro-Scale Optical Information Technology & Institute of Microscale Optoelectronics, Shenzhen University, Shenzhen 518060, China

*Corresponding author: cjmin@szu.edu.cn

**Corresponding author: xcyuan@szu.edu.cn

Received March 3, 2022 | Accepted June 17, 2022 | Posted Online July 12, 2022

The optical vortex beam has widely been studied and used because of its unique orbital angular momentum (OAM). To generate and control OAM in compact and integrated systems, many metallic metasurface devices have been proposed, however, most of them suffer from the low efficiency. Here, we propose and experimentally verify a high-efficiency monolayer metallic metasurface composed of semicircular nano-grooves distributed with detour phase. The metasurface can generate single or an array of OAM with spin-sensitive modulation and achieve the maximum efficiency of 60.2% in theory and 30.44% in experiment. This work has great potential in compact OAM detection and communication systems.

Keywords: optical vortex; orbital angular momentum; monolayer metallic metasurface.

DOI: 10.3788/COL202220.123601

1. Introduction

A vortex is a universal phenomenon in nature, and it also exists in light that is referred to as an optical vortex (OV)[1]. The OV was found to have a helical wavefront around a phase singularity and carry orbital angular momentum (OAM) during propagation[2]. Generally, OAM can exist in a variety of light beams such as the Laguerre–Gaussian beam[3], Bessel beam[4], and perfect vortex beam[5]. In theory, the topological charge of OAM can be arbitrary integers, and OV beams with different OAM are orthogonal to each other. Therefore, the OAM of OV beams can be regarded as a new degree of freedom and has great application prospects, especially in optical communication[6,7]. In addition, because of its unique characteristics in intensity and phase distributions, OV beams have been widely used in optical tweezers[8], nonlinear optics[9], optical imaging[10], and other fields.

With the development of applications of OV beams, various methods to generate and modulate OV have been proposed, including spiral phase plate[11], computed hologram[12], liquid crystal spatial light modulator[13], Q-plate method[14], and others. However, many traditional methods require large device size and complex optical system; thus, they are not suitable for applications of OVs in compact and integrated optical systems. To solve this problem, in recent years, many micro-nanoscale metasurface devices have been proposed for OV generation and modulation, such as metal nanoantennas, sandwiched meta-holograms, and silicon nano-columns[15–17]. However, there are some limitations in previously reported metasurfaces for application. For example, the early proposed transmission-mode metallic metasurface is easy to use and fabricate, but its efficiency is usually very low (less than several percent) due to the high reflection and absorption of metal[18,19]. Later, the reflective-mode metallic metasurface has been proposed to get a much higher efficiency of ~80%[15], but its sandwich structure (metal-dielectric-metal) brings higher requirements for fabrication[20]. Similarly, the all-dielectric metasurface usually has high efficiency due to the low-loss property of materials, but also has relatively high processing requirements for the large depth–width ratio of the dielectric unit structure[21]. Therefore, designing a metasurface with both high efficiency and low machining requirements remains a challenge.

In this Letter, a monolayer reflective-mode metallic metasurface structure is proposed and experimentally verified for high-efficiency generation and control of OV beams. The metasurface is designed with chiral unit structures of semicircular nano-grooves on a gold surface, which shows both high efficiency in reflected light and spin-dependent modulation on the reflection direction. The distribution of all nano-grooves on a gold surface is designed according to the detour phase principle[18], and thus any desired holographic phase can be generated by the metasurface to the reflected beam. We demonstrate that single OV beams or OV arrays can be generated by the metasurface, and it also can be used to detect both spin angular momentum (SAM) and OAM of incident light. Through theoretical and

experimental studies, we obtained the maximum efficiency of ~60.55% in theory and ~30.44% in experiment. Compared with many previously reported metallic metasurfaces, our proposed monolayer metasurface has much higher efficiency than the transmission-mode metallic metasurface and lower machining requirement than the sandwich-structured reflective-mode metallic metasurface. Thus, the proposed metasurface could provide a simple and high-efficiency solution for the generation and control of OV beams and promote its application in very compact and integrated optical systems.

2. Design Principle of the Metasurface

The schematic diagrams of the proposed metasurface structure and its working principle are shown in Fig. 1. Figure 1(a) shows the schematic diagram of the metasurface, which consists of an array of semicircular nano-grooves on a thick gold film and a glass substrate. A light is normally incident onto the metasurface, and, after being modulated by the phase hologram of the metasurface, the reflected light propagates to the left or right side depending on the right- or left-handed circular polarization of incident light, respectively, thus showing the spin-Hall effect of light[22].

The unit structure of the metasurface with parameters is presented in Fig. 1(b). The horizontal and vertical period lengths of the structural unit are P_x and P_y, respectively. The width of the semi-ring is w, the outer ring radius is r, the groove depth is h, and the thickness of the gold film is d. Here, the single semicircular groove can be regarded as a series of rectangular subgrooves that has well-known spin-dependent geometric phase, and thus a continuously varying geometric phase can occur along the semicircular groove, finally leading to the spin-Hall effect of the reflected light.

Figure 1(c) shows a schematic diagram of the detour phase principle based on the distribution of two adjacent grooves. Here each groove represents the single semicircular nano-groove shown in Fig. 1(b) that can be considered as an independent scatterer. After the light is incident into the two nano-grooves, diffraction light is emitted at each nano-groove, producing secondary waves like two point sources. When receiving the far-field diffracted light at a fixed angle θ, the optical path difference between the two wavefronts is $\Delta L = D \sin\theta$ (D is the distance between the two grooves), and the corresponding phase difference produced at that angle is $\Delta\varphi = 2\pi D \sin\theta/\lambda$ ($\lambda = 0.633$ μm is the incident wavelength). Thus, the phase difference can be controlled by changing the distance D. Through expanding the two grooves to a two-dimensional array of grooves with a horizontal period P_x and making $P_x = D = \lambda/\sin\theta$, we can achieve modulation of $\Delta\varphi$ in the range of $-\pi$ to π by just adjusting the position of the groove within each period P_x, as shown in the top of Fig. 1(c). Based on this principle, a two-dimensional phase hologram can be formed by choosing the positions of all grooves in each period of the proposed monolayer metallic metasurface and finally achieving holographic phase modulation on the reflected beam at the fixed angle θ[19].

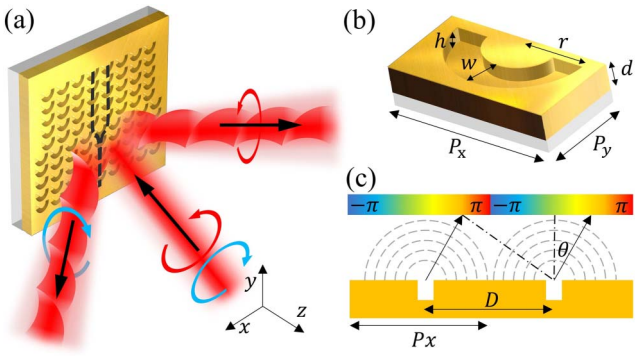

Fig. 1. (a) Schematic diagram of the proposed reflective-mode metallic metasurface structure. (b) Schematic diagram of the single unit structure of the metasurface with structural parameters. (c) Schematic diagram of the principle of detour phase.

In order to generate OAM in the reflected beam, a spiral phase distribution can be formed on the metasurface by the above-mentioned detour phase principle, and thus the distribution of semicircular nano-grooves on the gold surface looks like a fork grating[23], as the fork-shaped dashed lines shown in Fig. 1(a). Due to the functions of spiral phase modulation and spin-dependent reflection, a left-handed (right-handed) circularly polarized (LCP/RCP) plane-wave beam is normally incident onto the designed metasurface, and OAM can be generated in the left-side (right-side) reflected beam, respectively. Besides, detection for the OAM of the incident OV beam can also be realized by the metasurface with the reversed process[24].

3. Optimization of Unit Structure

In order to improve the performance of the metasurface, including the conversion efficiency of reflected light and the polarization extinction ratio (ER) of the two spin-polarized lights, several key parameters of unit structure are studied for optimization. As shown in Fig. 1(b), some parameters are fixed ($P_x = 0.896$ μm, $P_y = 0.4$ μm, $r = 0.4$ μm, $d = 0.2$ μm) according to the fabrication conditions, and the other two parameters of ring width w and groove depth h are studied for optimization. The 3D finite-difference time-domain (FDTD, Lumerical FDTD Solutions) simulation method was used to analyze the influence of the structural parameters on the polarization ER and conversion efficiency at the wavelength $\lambda = 0.633$ μm. Here, the polarization ER is defined as $\mathrm{ER} = 10\log\left(\frac{T_{+1}}{T_{-1}}\right)$, where T_{+1} and T_{-1} represent the energy of the far-field +1st and −1st diffraction orders [right and left side in Fig. 1(a)] of reflected light, respectively, which is used to quantify the spin-Hall effect under the incidence of LCP or RCP light. Figure 2(a) shows the ER results obtained by FDTD simulation under LCP incidence. It can be observed that the polarization ER is greater than 30 dB in most regions, and the maximum ER is about 70 dB. We also study the efficiency of the metasurface, which is defined as the percentage of the energy of the desired far-field +1st or −1st diffraction

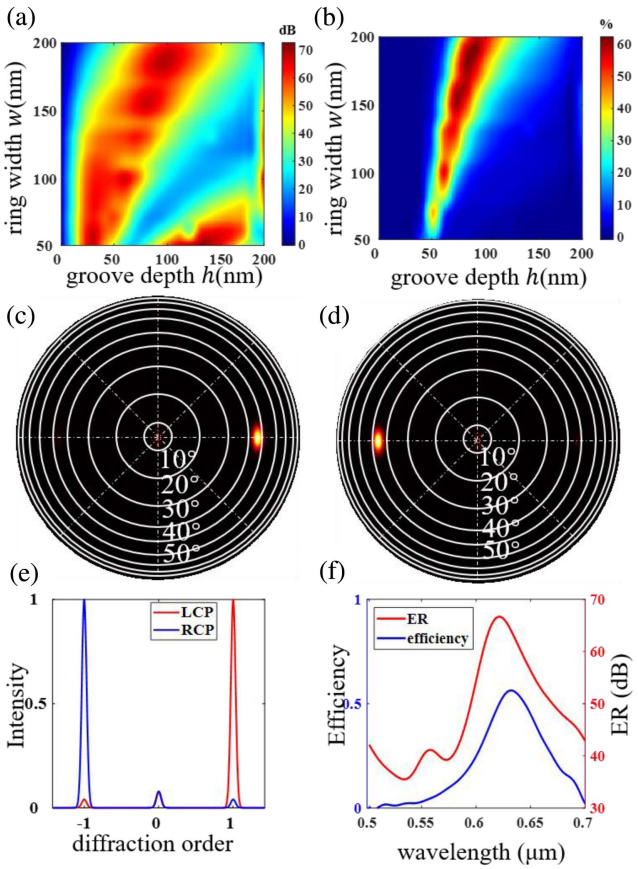

Fig. 2. Effect of ring width and groove depth on (a) the polarization ER and (b) the efficiency of the metasurface. Far-field distribution of the reflected light when the incident light is (c) LCP and (d) RCP with the optimized parameters. (e) Comparison of −1st, 0th, +1st diffraction order far-field intensity between LCP and RCP incidence. (f) The efficiency and ER as a function of incident wavelength.

order in the total energy of incident light. Figure 2(b) shows that the efficiency of the metasurface can reach more than 60% in some regions. To obtain both high polarization ER and large efficiency, we finally select the value of parameters as $w = 0.185\,\mu m$ and $h = 0.087\,\mu m$, with the corresponding optimized polarization ER of 63 dB and efficiency of 60.2%.

To demonstrate the performance of the optimized parameters, the FDTD simulated far-field distributions of the reflected light from the metasurface are shown in Figs. 2(c) and 2(d) for the incidence of LCP and RCP light, respectively. It can be observed that most reflected light propagates to the about 45° direction in the right side for the LCP case and the about −45° direction in the left side for the RCP case, verifying the expected spin-Hall effect. Here, the reflection angle θ (~45°) can be modulated by the period ($P_x = 0.896\,\mu m$) based on the principle in Fig. 1(c). The profiles of the above two cases in the far-field along the x axis are compared in Fig. 2(e), clearly presenting the intensities of −1st, 0th, and +1st diffraction orders in the far-field pattern. For the LCP/RCP case, the spin-selected reflection peak in the +1st/−1st diffraction order dominates the reflected light, while the other diffraction orders are strongly suppressed, verifying the high polarization ER of the optimized parameters. Figure 2(f) shows the performance of optimized parameters at different wavelengths. It can be found that the FWHM of the efficiency peak is about 60 nm, while the ER > 40 dB, and therefore our optimized metasurface has a certain working wavelength range.

4. Numerical Study on OAM Generation

According to the above-mentioned detour phase principle, spiral phase can be loaded on the metasurface to generate OAM in reflected beams. In Figs. 3(a) and 3(b), we show the FDTD simulated examples of OV beams with topological charge ($l = -1$ and $+1$) generated by the designed metasurface under RCP/LCP illumination, respectively. The metasurface has totally 55×123 structural units and is about $50\,\mu m \times 50\,\mu m$ in size. It can be seen that, when an RCP/LCP light is incident, the reflected light generates an OV with topological charge ($l = -1$ and $+1$) at the

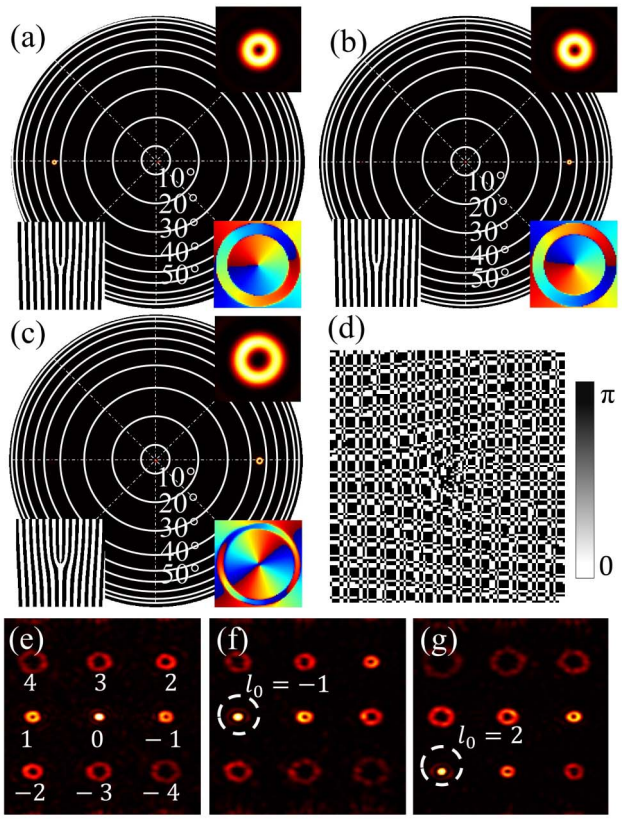

Fig. 3. Far-field distribution of the generated OV beam in the case of (a) RCP ($l = -1$), (b) LCP ($l = +1$), and (c) LCP ($l = +2$). The insets on the top-right corner, lower-left corner, and lower-right corner show the enlarged distribution of intensity, phase distribution on metasurface, and phase of the OV beam, respectively. (d) Phase distribution diagram of vortex Damman grating for 3×3 OV array. (e) 3×3 OV array with topological charges ranging from −4 to +4 is generated under LCP illumination. The modulated 3×3 OV array when the incident light is an OV beam with topological charge (f) $l_0 = -1$ and (g) $l_0 = +2$.

left/right side of the far-field as expected, showing the ring-shaped intensity distribution with the helical phase distribution covering $0–2\pi$. OV beams with other topological charge values can also be generated by changing the phase distribution on the metasurface. As shown in Fig. 3(c), an OV beam with topological charge ($l = +2$) is generated by the LCP incidence in the right side of the far-field reflected pattern, with an increased radius of the bright ring and helical phase distribution covering $0–4\pi$. The phase distributions loaded on metasurface are shown in lower-left corner of Figs. 3(a)–3(c), which all look like a fork grating. The phase of each unit structure in metasurface is determined by the position of each semicircular groove in the horizontal period as described in Fig. 1(c).

In addition to a single OV beam, an OV array with different OAMs can be generated by the designed metasurface, based on the principle of the two-dimensional Damman vortex grating[25]. By loading the phase distribution [Fig. 3(d)] of the two-dimensional Damman vortex grating on the metasurface with different positions of nano-grooves, a two-dimensional OV array with $M \times N$ orders can be formed in the right/left side of the far-field reflected pattern, under the incidence of LCP/RCP light, respectively. By designing the phase hologram of the Damman vortex grating, each OV in the $M \times N$ orders of the array can be controlled with different OAMs but equal energy. In Fig. 3(d), we show the FDTD simulated result of a 3×3 OV array with topological charges ranging from -4 to $+4$ under LCP illumination. The simulation structure contains 121×121 units, and the total size is about 100 μm × 100 μm. The center of the 3×3 OV array is a Gaussian point with topological charge of zero, and the radius of the OV ring increases with the larger topological charge of OAM.

If the incident beam is an OV beam with non-zero OAM, the diffraction order with the opposite OAM in the generated OV array will be restored from a ring-shaped distribution to a bright Gaussian point. Therefore, the designed metasurface device can also be used to detect the OAM of incident OV beams. In Figs. 3(e) and 3(f), we verify that when the incident OV beam has a topological charge of $l_0 = -1$ and $l_0 = +2$, the positions with topological charges of $l = +1$ and -2 in the OV array [Fig. 3(d)] are restored to Gaussian points, respectively. Moreover, because of the spin-Hall effect, the detection of SAM and OAM of incident light can be realized simultaneously in the metasurface, which have been proved to have great potential in cylindrical vector beam (CVB) and cylindrical vortex vector beam (CVVB) detection[19,26].

5. Experimental Verification

To verify the effectiveness of our designed metasurface, an experimental system is built, as schematically shown in Fig. 4(a). The light source is a He–Ne laser with wavelength $\lambda = 0.633$ μm. The laser beam first passes through lens L_1 and lens L_2 to collimate and expand the beam and then is converted into linear polarization through a polarizer. After passing through a rotatable 1/4 waveplate, the linearly polarized beam can be converted into an LCP or RCP beam. Next, the LCP or RCP beam is focused on the metasurface through a 5× objective lens. The metasurface-modulated light beam will be reflected to the direction of +45° (right side) or −45° (left side) and finally be recorded by CCD_1 and CCD_2, respectively, to verify the function of the metasurface. The metasurface sample was prepared on a double-polished glass substrate, then the gold film with thickness of 200 nm was evaporated on the glass substrate by electron beam evaporation, and finally the semicircular nano-grooves were etched on the gold film by the focused ion beam (FIB) method. The scanning electron microscope (SEM) image of the metasurface sample fabricated is presented in Fig. 4(b), showing the array of semicircular nano-grooves on gold surface. The number of units in the metasurface was 30×60 with the total size of about 30 μm × 30 μm, and all structural parameters were chosen from the optimized numerical results (Fig. 2).

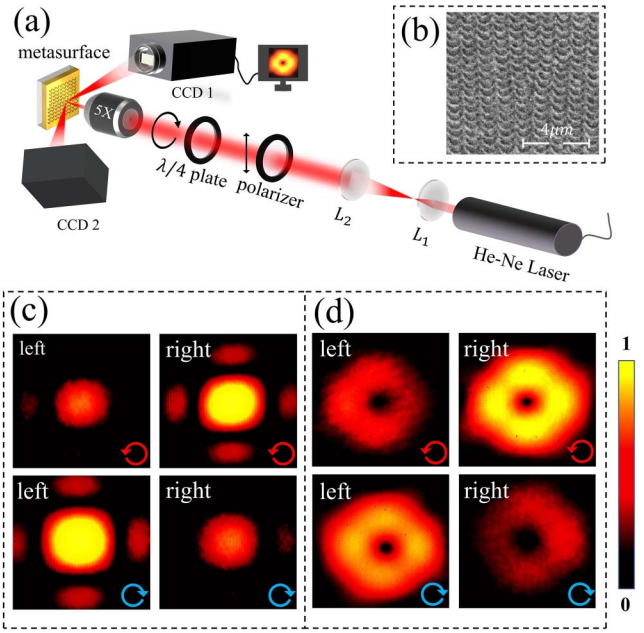

Fig. 4. (a) Schematic diagram of the experimental system. (b) SEM image of the metasurface sample. Comparison of experimental results of left-/right-side reflected pattern under LCP/RCP incidence with (c) the uniform grating structure of semicircular nano-grooves and (d) the metasurface structure to generate OV beams with topological charge $l = 1$.

The experimental measurements of two different structures of metasurfaces were performed, including a uniform grating structure of semicircular nano-grooves and a spiral phase metasurface structure to generate OV beams with topological charge $l = 1$ [sample in Fig. 4(b)]. Figure 4(c) shows the experimental results of reflected beam in both +45° and −45° angle directions under LCP and RCP illumination onto the uniform grating structure. It can be observed that under the incidence of LCP light, the reflected light produces a bright light spot on the right side and a much lower spot on the left side, in agreement with the theoretical predictions in Fig. 2(c). The measured efficiency of the bright spot energy on the right side in respect to the total incident light energy is about 25.56%, while the weaker spot on the left side

has the efficiency of 4.59%, so the desired diffraction light (right side) is about 5.6 times more than the undesired part (left side). On the contrary, when the incident light is changed to RCP, the bright spot appears on the left side of the far-field pattern with the efficiency of 30.44%, and the weaker spot appears on the right side with the efficiency of 4.94%, demonstrating a contrast of about 6.2 times. These efficiency values are much higher than that of many previously reported transmission-mode metallic metasurfaces (usually less than several percent)[17–19]. For the other metasurface sample with a spiral phase modulation [Fig. 4(d)], the experimental results are similar to that in Fig. 4(c), except that all light spots are modulated to a donut-shaped OV pattern. For the generated OV beams, the measured efficiency is about 10.78% (right side) and 2.06% (left side) for the LCP case, and 1.97% (right side) and 11.01% (left side) for the RCP case, respectively, both showing the contrast more than five times. These experimental results verify that the designed metasurface can realize spin-selected generation of OV beams.

It is noted that the experimental results of both the efficiency and polarization ER are not as good as the theoretical results shown in Fig. 2, mainly due to the limited machining precision in FIB fabrication of the metasurface samples.

6. Conclusion

In conclusion, we numerically study and experimentally verify the monolayer reflective-mode metallic metasurface for high-efficiency generation and control of OAM beams. The metasurface is composed of semicircular nano-grooves on a gold surface distributed with the detour phase principle. After optimization of the structural parameters, the metasurface shows both high efficiency in generated light and spin-dependent modulation on the reflection direction. A single OV beam and OV array can be generated by the metasurface, and it also can be used to detect both SAM and OAM of incident light. The proposed metasurface device shows advantages of high efficiency, easy fabrication, and very compact size, thus having great potential in applications such as integrated OAM/CVB detection and communication systems.

Acknowledgement

This work was partially supported by the Guangdong Major Project of Basic and Applied Basic Research (No. 2020B0301030009), National Natural Science Foundation of China (Nos. 62175157, 61935013, 61975128, and 62105219), Leading Talents of Guangdong Province Program (No. 00201505), Natural Science Foundation of Guangdong Province (No. 2019TQ05X750), and Shenzhen Science and Technology Program (Nos. JCYJ20180507182035270, RCJC20210609103232046, JCYJ20210324120403011, and KQTD20170330110444030).

References

1. A. M. Yao and M. J. Padgett, "Orbital angular momentum: origins, behavior and applications," Adv. Opt. Photonics **3**, 161 (2011).
2. Y. Bai, H. Lv, X. Fu, and Y. Yang, "Vortex beam: generation and detection of orbital angular momentum [Invited]," Chin. Opt. Lett. **20**, 012601 (2022).
3. M. W. Beijersbergen, L. Allen, H. E. L. O. Vanderveen, and J. P. Woerdman, "Astigmatic laser mode converters and transfer of orbital angular-momentum," Opt. Commun. **96**, 123 (1993).
4. J. Arlt and K. Dholakia, "Generation of high-order Bessel beams by use of an axicon," Opt. Commun. **177**, 297 (2000).
5. Y. Zhang, W. Liu, J. Gao, and X. Yang, "Generating focused 3D perfect vortex beams by plasmonic metasurfaces," Adv. Opt. Mater. **6**, 1701228 (2018).
6. N. Bozinovic, Y. Yue, Y. Ren, M. Tur, P. Kristensen, H. Huang, A. E. Willner, and S. Ramachandran, "Terabit-scale orbital angular momentum mode division multiplexing in fibers," Science **340**, 1545 (2013).
7. J. Fan, J. Zhao, L. Shi, N. Xiao, and M. Hu, "Two-channel, dual-beam-mode, wavelength-tunable femtosecond optical parametric oscillator," Adv. Photonics **2**, 045001 (2020).
8. D. G. Grier, "A revolution in optical manipulation," Nature **424**, 810 (2003).
9. X. Fang, H. Yang, W. Yao, T. Wang, Y. Zhang, M. Gu, and M. Xiao, "High-dimensional orbital angular momentum multiplexing nonlinear holography," Adv. Photonics **3**, 015001 (2021).
10. C. Zhang, C. Min, L. Du, and X. C. Yuan, "Perfect optical vortex enhanced surface plasmon excitation for plasmonic structured illumination microscopy imaging," Appl. Phys. Lett. **108**, 201601 (2016).
11. M. W. Beijersbergen, R. P. C. Coerwinkel, M. Kristensen, and J. P. Woerdman, "Helical-wavefront laser beams produced with a spiral phaseplate," Opt. Commun. **112**, 321 (1994).
12. N. R. Heckenberg, R. McDuff, C. P. Smith, and A. G. White, "Generation of optical phase singularities by computer-generated holograms," Opt. Lett. **17**, 221 (1992).
13. M. Chagnon, M. Osman, Q. Zhuge, X. Xu, and D. V. Plant, "Analysis and experimental demonstration of novel 8PolSK-QPSK modulation at 5 bits/symbol for passive mitigation of nonlinear impairments," Opt. Express **21**, 30204 (2013).
14. L. Marrucci, C. Manzo, and D. Paparo, "Pancharatnam-Berry phase optical elements for wave front shaping in the visible domain: switchable helical mode generation," Appl. Phys. Lett. **88**, 221102 (2006).
15. G. Zheng, H. Muhlenbernd, M. Kenney, G. Li, T. Zentgraf, and S. Zhang, "Metasurface holograms reaching 80% efficiency," Nat. Nanotechnol. **10**, 308 (2015).
16. J. Liu, C. Min, T. Lei, L. Du, Y. Yuan, S. Wei, Y. Wang, and X. C. Yuan, "Generation and detection of broadband multi-channel orbital angular momentum by micrometer-scale meta-reflectarray," Opt. Express **24**, 212 (2016).
17. N. Yu, P. Genevet, M. A. Kats, F. Aieta, J. P. Tetienne, F. Capasso, and Z. Gaburro, "Light propagation with phase discontinuities: generalized laws of reflection and refraction," Science **334**, 333 (2011).
18. C. Min, J. Liu, T. Lei, G. Si, Z. Xie, J. Lin, L. Du, and X. Yuan, "Plasmonic nano-slits assisted polarization selective detour phase meta-hologram," Laser Photonics Rev. **10**, 978 (2016).
19. Y. Fu, C. Min, J. Yu, Z. Xie, G. Si, X. Wang, Y. Zhang, T. Lei, J. Lin, D. Wang, H. P. Urbach, and X. Yuan, "Measuring phase and polarization singularities of light using spin-multiplexing metasurfaces," Nanoscale **11**, 18303 (2019).
20. S. Chen, Z. Xie, H. Ye, X. Wang, Z. Guo, Y. He, Y. Li, X. Yuan, and D. Fan, "Cylindrical vector beam multiplexer/demultiplexer using off-axis polarization control," Light Sci. Appl. **10**, 222 (2021).
21. M. Khorasaninejad, W. T. Chen, R. C. Devlin, J. Oh, A. Y. Zhu, and F. Capasso, "Metalenses at visible wavelengths: diffraction-limited focusing and subwavelength resolution imaging," Science **352**, 1190 (2016).
22. K. Y. Bliokh, F. J. Rodríguez-Fortuño, F. Nori, and A. V. Zayats, "Spin–orbit interactions of light," Nat. Photonics **9**, 796 (2015).
23. Z. Xie, S. Gao, T. Lei, S. Feng, Y. Zhang, F. Li, J. Zhang, Z. Li, and X. Yuan, "Integrated (de)multiplexer for orbital angular momentum fiber communication," Photonics Res. **6**, 743 (2018).
24. T. Lei, M. Zhang, Y. Li, P. Jia, G. N. Liu, X. Xu, Z. Li, C. Min, J. Lin, C. Yu, H. Niu, and X. Yuan, "Massive individual orbital angular momentum channels for multiplexing enabled by Dammann gratings," Light Sci. Appl. **4**, e257 (2015).
25. S. Gao, T. Lei, Y. Li, Y. Yuan, Z. Xie, Z. Li, and X. Yuan, "OAM-labeled free-space optical flow routing," Opt. Express **24**, 21642 (2016).
26. J. Fang, Z. Xie, T. Lei, C. Min, L. Du, Z. Li, and X. Yuan, "Spin-dependent optical geometric transformation for cylindrical vector beam multiplexing communication," ACS Photonics **5**, 3478 (2018).